

2012 ASME Human Powered Vehicle Challenge  
April 27-29, 2012  
Grove City College  
Grove City, PA

# Design Report

## 2012 Human Powered Vehicle *Seabagel*

Franklin W. Olin College of Engineering



Team Leaders: Eric Jones and Jackie Rose

Team Members: Alex Niswander, Travis Schuh, Meghan Murray, Ben Smith, Andrew Carmedelle, Heidi Nafis, Molly Farison, Ben Chapman, Dan Kearney, Orion Taylor, Juliana Nazare, Cypress Frankenfeld, Nick Eyre, David Pudlo, Gaby Waldman-Fried, Maggie Su, Kari Bender, Janie Harari, Jay Patterson, Kaitlin Gallegher, Sophia Utset-Ward

## Table of Contents

Abstract.....	3
Design.....	3
Design Introduction.....	3
Slow Speed Stability System (SSSS) Design Methodology.....	5
Design Goals and Objectives .....	5
Actuation Design.....	6
Drivetrain Design Methodology.....	7
Technology Innovation: Rider Variation Compensation System .....	8
Background and Justification .....	8
Design Goals .....	8
Preliminary Designs .....	8
Final Design.....	9
System Overview .....	9
Dealing with Singularities and Over-constraints.....	10
Pedal Adjustment Mechanism.....	10
Strength Testing of Crank Connector.....	11
Innovation.....	12
Analysis .....	13
Rollover Protection System.....	13
Aerodynamics: Fairing Profile .....	14
2D Testing.....	16
Iterating upon Wedge.....	18
Crosswind Analysis.....	19
Interchange Strength Analysis.....	20
Testing .....	21
Rollover Protection System.....	21
Developmental Testing.....	23
Composite Rib Shape.....	23
Rider Confidence Testing.....	24
Performance Testing.....	25
Interchange Strength Testing.....	25
Rider Adjustment Testing .....	26
Safety .....	27
Appendix.....	29
Appendix A. Cost Analysis .....	29
Appendix B. Engineering Drawings.....	31

## **Abstract**

The Olin College Human Powered Vehicle Team is returning to the ASME Human Powered Vehicle Challenge for the seventh year. With knowledge that all vehicles would participate in an event similar to the utility class from previous years, our specific goals for this year were to design a much more practical vehicle, improve reliability, and increase rider confidence through intuitive design. These goals come along with the standards our team always uses as benchmarks: we strive to design and build a fast and agile vehicle that all members of our team can comfortably ride. Using knowledge gained from previous experiences at the ASME HPVC, the 2012 competition vehicle, *Seabagel*, incorporates the following innovations to achieve our goals:

1. While past vehicles have included an adjustable seat to accommodate differences in rider height, adjustment on *Seabagel* is achieved by adjusting pedal location. This ensures a comfortable fit for all riders while also allowing the window and roll protection system to be designed with confidence that each rider's torso will remain in the same place regardless of rider height.
2. *Seabagel* is a fully-faired vehicle able to start and stop without assistance. A custom designed and fabricated mechanical system allows the driver to pull one lever on the handlebars in order to both lower and raise the slow speed stability system.
3. Significant improvements in fairing construction techniques have created a safer and more practical vehicle. This year's fabrication methods include more extensive use of vacuum bagging to achieve a predictable shape and professional finish. The fairing seam also includes a new attachment technique. These improvements also allow the use of an integrated composite structure as our rollover protection system, saving both weight and space.

## **Design**

### **Design Introduction**

*Seabagel* was designed and fabricated for the 2012 ASME HPVC. Many of the vehicle's systems have changed dramatically from our previous entries, due not only to the new competition rules, but also to our team's commitment to annually evolve and innovate.

After seeing Sam Whittingham's *Varna Tempest* displayed at Indianapolis Motor Speedway last year, our team was inspired to make a monocoque vehicle. Since the two largest contributors to vehicle weight in past years have been the structural steel frame and the fairing, a fabrication technique that allows for structural use of composite material drastically decreases overall weight. To compensate for the structural stability normally provided by the frame, we have added strength-tested carbon fiber ribbing.

Our fairing fabrication techniques have also improved over previous methods. After years of experimental mold-making techniques, last year's vehicle, *Shadowfax*, benefitted greatly from the precision made possible by using a solid foam male mold. Because we were determined to build a monocoque vehicle this year, we further built upon these methods when building

*Seabagel's* fairing. Our team was granted access to a CNC router, which allowed us to quickly cut a foam male plug to the exact desired shape. This mold has a finish of 1/10 inch steps, as seen in Figure 1, which allows sanding – a previously time-consuming process – to be trivial. More importantly, faster mold fabrication allows a stronger focus on using robust processes to make a professional quality fairing.

We tested the complete mold making process by making a 1/3 scale model of our fairing. We first created a foam male plug and did four layups on it, one on each quarter of the plug, in order to make four female molds. We then bolted the female molds together in pairs to create two half molds. We did a final layup on the two molds and used a vacuum bagging technique to produce a fairing that is of the desired shape and has a professional finish on the outside surface. We are currently in the process of fabricating the fairing for *Seabagel*, and we do not anticipate any major problems in scaling up the process.



Figure 1: CNC foam pieces forming the male mold. Note that the mold is upside-down in this picture.

While the final fairing profile for *Seabagel* is similar to that of *Shadowfax*, it is an original design achieved through iterative analysis using STAR-CCM+, a professional CFD package. A complete fairing profile analysis is included later in this report. Our iterative design process and detailed analysis on variables including length, tail box concavity, and wheel box shape have substantially optimized the fairing profile for *Seabagel* for speed, within the design constraints placed on it by other vehicle systems.

In accordance with our monocoque structural design, we are moving away from a steel roll hoop and integrating our rider protection system into the fairing in the form of strengthened composite construction. Our rollover protection system will be completely integrated into the fairing and will reduce the mass of the vehicle. Intensive ribbing and adding additional layers to the external shell, along with installing load bearing interface points between top and bottom halves of the fairing, will allow our removable top half to provide the necessary resistance to impacts. When carbon fiber is given additional geometry through ribbing (constructed by laying up over lengths of foam), it gains enough strength to protect against crushing, such that it can support the mandated loads in a similar fashion to a roll hoop.

New to the 2012 HPVC, all vehicles must be capable of starting and stopping without assistance. Since in past years drivers relied on teammates to catch the vehicle as it slowed to a stop, we needed to design a system to keep riders balanced at slow speeds. We implemented a Slow Speed Stability System (SSSS) consisting of rollerblade wheels mounted on the ends of sliding rods positioned on both sides of the vehicle. Our deployment method, a simple mechanical system actuated by a single lever on the handlebars, makes the SSSS both reliable and convenient. Further information regarding design methods and considerations concerning the Slow Speed Stability System are included later in this section.

A reliable drivetrain system is a cornerstone in *Seabagel's* performance. Full analysis of custom drivetrain components is included later in this report. In addition to *Seabagel's* crank arms and interchange, we departed from standard cycling bottom brackets in exchange for billet crank shafts with inlaid bearings, both of which reduce the tread of the cranks. A wide range of speeds is achieved through a two-stage chain reduction and a derailleur mounted on the wheel. This system benefits from the modular frame jig we first used to fabricate *Shadowfax*. This frame jig helped fabricate a planar drive system, supplemented by large chain guards to help correct for the twist induced by both steering and driving with the front wheel. This drivetrain is expected to have few reliability issues.

Our team always strives to design a vehicle that everyone on the team can ride. As our riders heights span more than one foot, it is necessary to have a system to compensate for these differences. While all of our previous vehicles have used an adjustable seat, this year's vehicle instead utilizes a set of adjustable pedals. This radical departure from our standard design is beneficial in ways beyond accounting for different drivers, and is explained in detail in the Technology Innovation Section.

## **Slow Speed Stability System (SSSS) Design Methodology**

### *Design Goals and Objectives*

At the 2011 ASME HPVC East, our team observed the handiwork of other teams who had incorporated a landing gear system into their vehicle designs. Each design was similar – the driver could actuate a mechanism to lower one or two rollerblade wheels out of the fairing to the ground, creating a tripod holding the vehicle upright.

For our design, we focused on reliability and ease of use for the driver. First we studied the simple statics of where to add support to the vehicle by adding wheels to previous vehicles at a variety of heights, widths, and positions along the frame. This enabled us to determine how wide and how far behind the rider the wheels would need to be in order to successfully stabilize the vehicle at low speeds. We found that a narrow wheelbase was needed, so we did not need to design a mechanism that extends wider than our fairing.

Secondly, we wanted to ensure that the driver can actuate the system without losing control of the vehicle because the vehicle is most unstable at these slow speeds. We found that an ideal system would be actuated completely by one lever on the handlebars. This would give the driver the greatest ease of use, as there would be no requirement for any actions other than the instinctive pull of a brake lever, and it does not require the driver to remove his or her hands

from the handlebars. The most notable drawback of the brake lever is that the achievable travel on the actuation line is only a few inches. We chose to amplify this motion by using it to extract power from the drivetrain.

Third, we were concerned about weight of the system and discussed adding a triangulating wheel to only one side of the vehicle rather than both sides. While this option would significantly cut the weight, we felt that it would also severely limit the ease of use for the system. Requiring the driver to always lean to one side when stopping is not practical, as doing so is difficult during sudden stops or when stopping on inclined surfaces. For these reasons, we designed our system to triangulate on either side of the vehicle.

### *Actuation Design*

The Slow Speed Stability System consists of rollerblade wheels mounted on the ends of extending rods. By pulling a lever just a few inches, the system is able to deploy or retract. An important constraint is that both the deployed and retracted positions should be locked. A failed lock on the deployed system would be a critical failure and the vehicle would fall. Similarly, a failed lock in the retracted position could severely limit the turning radius on the vehicle and prohibit high speed maneuvering. As with all systems, weight was a major concern. After deliberating with this issue and the constraints, we arrived at a two-part system that incorporates spring tensioned rods and a ratchet and pawl mechanism for locking the system in place.

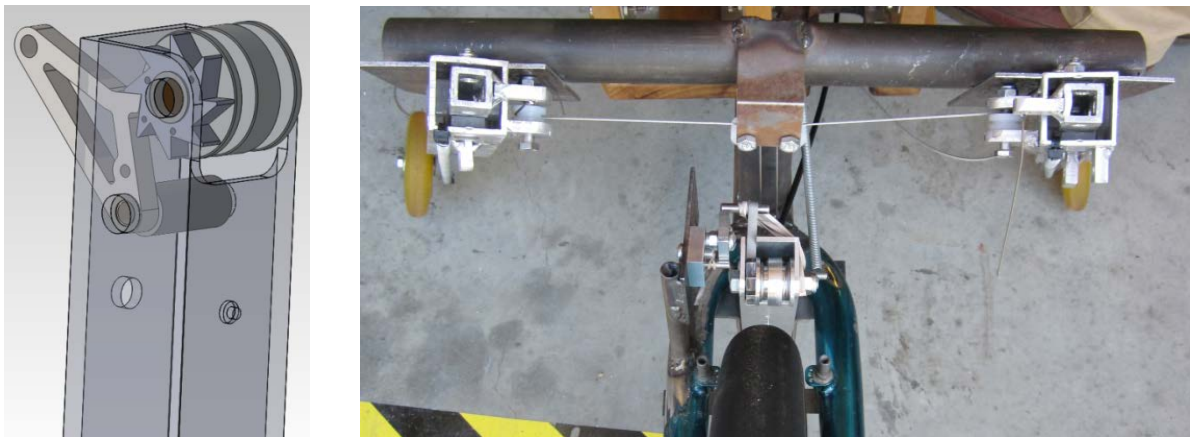


Figure 2: (a)The custom ratcheting power take-off and (b)the full prototype of the Slow Speed Stability System

The design for the ratcheting system is shown in Figure 2(a). When the driver pulls on a brake lever, the ratcheting assembly tilts to contact the rear wheel. The rear wheel spins the ratchet forward, which pulls cables attached to the upper portion of the rods and deploys the landing gear. When the driver releases the lever, the pawl holds the ratchet in place, thereby locking the system in the deployed position. The next time the rider pulls on the brake lever, a one-way trip mounted in the travel path of the pawl releases the pawl, allowing the system to retract. This method does not require the rear wheel to be in contact with the system when the driver is trying to stow the Slow Speed Stability System. A prototype of this system can be seen in Figure 2(b).

## Drivetrain Design Methodology

The drivetrain design requirements include reliability, effectiveness at varying speeds, efficiency, and compactness. We chose front-wheel drive over rear-wheel drive because the latter necessitates a taller fairing in order to keep the chain off the bottom of the fairing. Our experience has also shown that a properly designed front wheel drive can be as reliable as a rear wheel drive. Therefore, we focused on designing a proper front-wheel drive system.

A key insight in our drivetrain design was that we did not need the same number of gears found in a standard eight-speed cassette provided that we could match the same speed range. This freed us to use solutions other than a conventional bicycle drivetrain. Based on previous experiences and the observation of other front-wheel drive vehicles, we perceived that it was important for reliability to have the chain as close to the axis of rotation as possible and with the smallest possible jog between the two sprockets. From this, we produced seven ideas:

1. A design to replace the shifting function usually performed by a derailleur with a four-speed dogged transmission. This design would allow us to maintain a constant chain line, having the added benefit of being able to shift from a stop and being more reliable overall.
2. A triangle of sprockets spaced around an input shaft with three different gear ratios. The system would shift by rotating the triangle and changing which sprocket engaged with the output chain.
3. A two-stage reduction with a cassette and a set of four chainrings at the beginning of the second stage (placed near the head tube) for shifting.
4. A standard triple chainring arrangement on the cranks.
5. An internal hub at the wheel, such as a NuVinci hub.
6. A two-stage reduction with shifting at the wheel.
7. A two-stage reduction with shifting at the second sprocket in the first reduction.

To decide between ideas, we created a design table to compare designs against our goals and requirements for the drivetrain, found in Table 1. We ultimately settled on a design with a derailleur and cassette at the wheel because it offers a simple, reliable solution.

	Four-speed dog	Sprocket Triangle	Shift at top, tension at bottom	Shift at cranks w/ triple	Internal hub	Shifter at wheel	Shift at second gear in first chain
Manufacturability	2	4	3	5	5	4	4
Light Weight	2	4	5	5	2	5	5
Simplicity	2	3	3	4	4	4	3
Reliability (2x)	10	3	7	8	8	7	7
Flexibility	4	5	5	2	5	5	5
Cost	3	4	4	4	1	5	5
Innovation	5	5	3	2	1	2	2
	<b>28</b>	<b>28</b>	<b>30</b>	<b>30</b>	<b>26</b>	<b>32</b>	<b>31</b>

Table 1: Drivetrain Design Table

## **Technology Innovation: Rider Variation Compensation System**

### **Background and Justification**

Each year, we design our vehicle so that each team member can comfortably ride. As our riders' heights span over one foot, we needed a mechanical system to adjust for each rider.

Accomplishing this task has normally involved integrating a movable seat, but this year we designed a system that moves the pedal location forward and backward with respect to a stationary driver. In a utilitarian setting, easily adjustable pedals would allow for all members of a family to operate the same vehicle, as opposed to each member owning their own bicycle.

The advantages of keeping different riders in the same location span far beyond practical purposes. Because different riders occupy the same space inside the fairing, all riders' shoulders are located in the same vertical plane. Thus the widest point of our fairing is concentrated in a small section of the fairing's length, allowing for a more streamlined shape. Additionally, because all riders' heads are in similar locations, our window is more effective for all riders. This enables easier fabrication and improved aerodynamics. An added safety benefit is that riders are centered within the roll bar. In previous vehicles, a shorter rider could contact the ground in the event of an un-faired rollover because the roll bar was located behind her at the widest point on the fairing. This new system enables our vehicle to implement a rollover protection system that protects all riders equally, increasing safety and boosting driver confidence.

### **Design Goals**

The rider variation compensation system had to be designed to accommodate the 6.25 inch variation in our riders' ideal pedal positions. The system also has to allow for riders to be switched with minimal time added to pit stops for pedal changes. Finally, we required that the reliability and power transfer of the drivetrain not be compromised by the system.

### **Preliminary Designs**

In creating the configuration of our compensation system, we started with three main designs, shown in Figure 3. The first involved a telescoping frame tube allowing the pedals to extend away from the rider. The second system configuration used a pivoting frame tube to swing the bottom bracket and pedals away from the rider. Our final system used two sets of crank arms in a four-bar linkage with pedals mounted on the connecting arms enabling the pedals to be moved to adjust for rider height. Using the design table presented in Table 2, we opted to move forward with the design of the four-bar linkage because it was the most mechanically sound system.



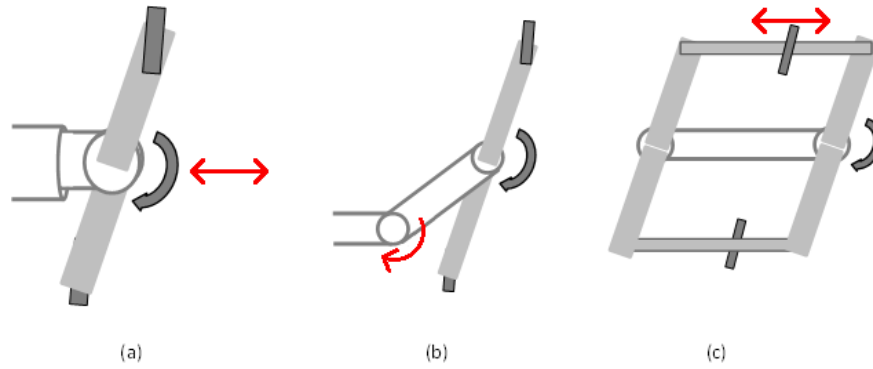


Figure 3: Designs considered for achieving adjustability at the pedals

Requirement	Telescoping	4-Bar Linkage	Swing Arm	Standard Cranks
Accommodate rider differences (2x)	5	5	3	1
Rider change time	3	5	3	5
Reliability (2x)	2	5	5	5
Power Transfer	4	4	4	5
	<b>21</b>	<b>29</b>	<b>23</b>	<b>22</b>

Table 2: Design Table for Adjustable Cranks. Each design was ranked on a scale of 1 (worst) to 5 (best) with regard to each requirement. The score is the weighted sum for each design.

## Final Design

### System Overview

The system can be seen in Figure 4. The system consists of two sets of cranks spaced 11 inches apart. An arm spans the cranks on each side of the vehicle’s frame. The pedals are mounted to a block that slides along the arm and is constrained at discrete points by a spring-loaded pin. Pedal adjustment occurs by retracting the pin, sliding the pedal, and releasing the pin. To expedite adjustment and reduce the risk of locating the left and right pedals in different locations, we engraved a numbered index in the arm at each position.



Figure 4: The rider compensation system mounted on Charlie, our current prototype.

### *Dealing with Singularities and Over-constraints*

The four-bar linkage system has two major issues that had to be avoided. The first is the singularity created when both sets of cranks are horizontal. At this point, there is nothing in the system to keep both sets of cranks rotating in the same direction. Thus, the system runs the risk of becoming catawampus without another constraint. To force the cranks to rotate consistently in the same direction, we implemented a timing belt system running between the sets of cranks, seen in Figure 5. The load needed to keep the cranks synchronized is small; we chose a timing belt, rather than a chain, because the belt is lighter weight and more efficient.



*Figure 5: The timing belt mounted to achieve constant forward rotation.*

The second issue with a four-bar linkage is that it is over-constrained in its base state. To add the necessary degrees of freedom, we slotted each crank connecting arm at one end. This allows the crank connector to slide with respect to the cranks. An exploded view of the slot can be seen in Figure 6.

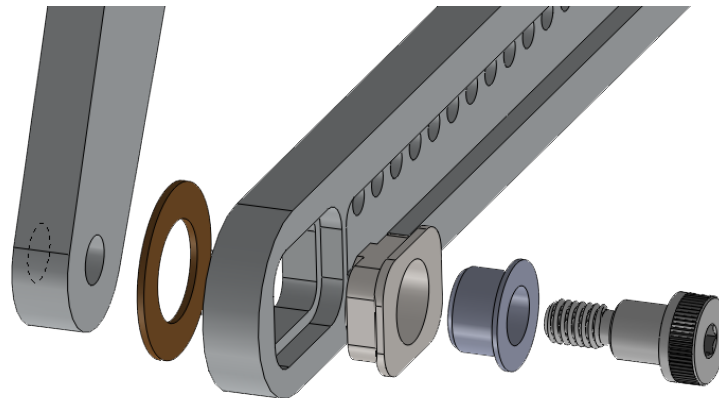


*Figure 6: A slot in the crank connecting arm adds a degree of freedom.*

### *Pedal Adjustment Mechanism*

*The pedal adjustment mechanism needs to be robust to transfer the stalled load of a pedal stroke but also be slender enough to not increase the tread of the cranks. In our final design, which can be seen in*

Figure 7, the pedal is mounted in a sliding block. The block slides in a flanged slot, constraining moments and non-forward loads, while a spring-loaded pin sets the leg extension length for the driver and counters standard pedaling forces.

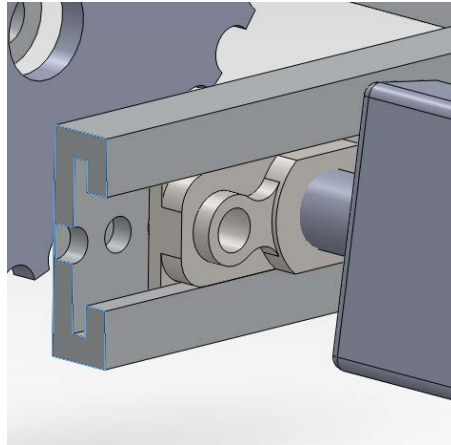


Figure 7: Cut-away view (highlighted in blue) of the pedal adjustment mechanism.

### Strength Testing of Crank Connector

The two most concerning failure modes were the shearing of the pin and the plastic deformation of the flange. With knowledge that the yield strength of steel is 36ksi<sup>1</sup>, we can calculate the proper pin diameter,  $D$ , with a factor of safety of two:

$$\sigma_{yield} = \frac{F}{A} = \frac{4F}{\pi D^2} \quad D = \sqrt{\frac{4 * F * FoS}{\pi * \sigma_{yield}}} = \sqrt{\frac{4 * 250lbs * 2}{\pi * 36ksi}} = .133in$$

From these calculations, we find that the pin diameter must be at least 0.133in. Our quarter inch pin will counter the load of the rider with a factor of safety of seven.

Because the flange is only 3/16 inch thick, we were concerned that it may permanently deform while counteracting the coupled forces applied by the pedal block on the arm. To minimize these forces, we lengthened the span of the tabs on the pedal block. Finite element analysis (FEA) was used to verify that the designed crank connecting arm was sufficient. To test the load, one end of the crank connecting arm was fixed while the other was allowed to slide in a plane, as constrained in the physical system. Applying a 250lb load at the location of the pedal's center outputs the results seen in Figure 8(a). The highest von Mises stress occurs at the thin backing to the pin's pocket, and even this non-critical area has a factor of safety over four.

<sup>1</sup> Philpot, Timothy A. *Mechanics of Materials*. John Wiley and Sons, Inc. Hoboken, NJ. 2008.

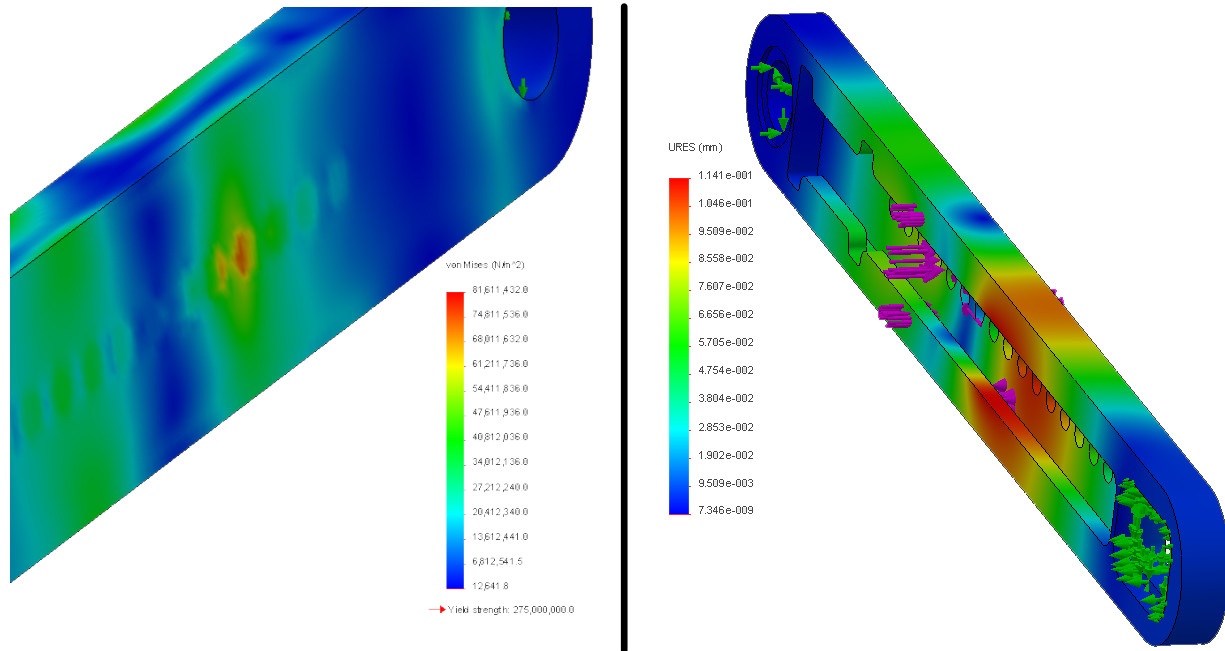


Figure 8: FEA results for the Crank Arm showing (a) von Mises stress, and (b) displacement.

This large factor of safety means that we have the option of downsizing these crank connectors to save weight. However, large displacements in components of the system could create inefficiencies. Therefore, the rigidity of the system is valued over the potential weight savings. From the FEA results shown in Figure 8(b), the maximum displacement of the crank connecting arm is 0.005 inches. Because the crank connectors' maximum deformation during operation is on the same order of magnitude as the tolerances we can hold during machining, inefficiencies due to deformation will be no larger than those due to fabrication imperfections. Thus, we do not expect our pedal adjustment system to contribute significant power losses under load.

## Innovation

This method of pedal adjustment employs standard mechanisms in a progressive way. While other teams in previous years have attempted adjustable pedal position, none have succeeded to our knowledge. In the past we have incorporated adjustment in our seat, but such a system led to the problems described above. This new system provides a rigid means of rider variation compensation while avoiding the flaws associated with other means of adjustment. The simplicity of our system makes it comparable to other adjustment systems, and makes it possible for this new innovation to be widely accepted.

This system of rider variation compensation holds promise in the commercial market of velomobiles and human powered vehicles because of its high degree of effectiveness. In the current bicycle usage paradigm, each member of a family owns a bicycle, largely because this is required for correct fit. Adjusting the seat height of an upright bicycle can make for awkward rides if the user is not properly sized for the vehicle. However, a recumbent with this innovative pedal adjustment system will fit most riders between 4'10" and 6'3" because the seat and steering systems remain usable by riders regardless of size.

Since this innovation makes the recumbent bicycle accessible to a larger variety of riders, it is quite useful and marketable. The simplicity and ease of use that this feature enables riders of all sizes, knowledge, and skill level to use the vehicle comfortably. As a team, we would have no problem spending extra money on this device, as we have riders of various sizes and it has proven difficult adjusting the vehicle otherwise. We believe the whole human-powered vehicle community can benefit from this adjustment system, because by comfortably accommodating multiple drivers, recumbent bicycles move one step closer to the car-replacement paradigm.

## Analysis

### **Rollover Protection System**

Since our RPS is a departure from what we have done for the past five years and we have little prior experience with structural composites, it was crucial that we perform analysis in addition to testing in order to validate our concept. We used the composite analysis feature of the SolidWorks Premium Simulation package to analyze our top shell under a top and side load, per specification of the 2012 ASME HPVC rules.

For material properties of carbon fiber, we used the Standard Uni-Directional Carbon Fiber strength characteristics provided by Performance Composites, which reports a Young's Modulus of 135 GPa in the axial direction, a Poisson's ratio of 0.30, and an Ultimate Tensile Strength in the axial direction of 1500 MPa<sup>2</sup>. We used a two ply layup with one direction aligned with the front-rear axis of the vehicle and the other direction aligned along the hoop axis of the fairing. Based on test layups, we measured the thickness of each layer of carbon to be 0.015 inches.

We tested two load conditions, a 600lb-f top load at 12° from vertical and a 300lb-f side load. The results are shown in Figure 9 to Figure 11. This model predicts that we are well below the yield strength of both the carbon fiber and the cross brace tube in both cases. The model does predict that we are above the maximum allowable deformation under the side load condition, yet the model does not include the strength that will be added by our lip and other internal reinforcements so we expect to see deformations that are below the allowable deformation once we complete fabrication of the fairing. While the model predicts a large factor of safety, it does not account for secondary failure modes like abrasion of the rollover protection system or buckling of the surface. For these reasons, we will build in rib reinforcements around the rider and in places where we expect high stress. Our main conclusion from these results is that there is enough strength inherent in the material of our RPS, provided that we can prevent buckling and protect against abrasion.

---

<sup>2</sup> [http://www.performance-composites.com/carbonfibre/mechanicalproperties\\_2.asp](http://www.performance-composites.com/carbonfibre/mechanicalproperties_2.asp)

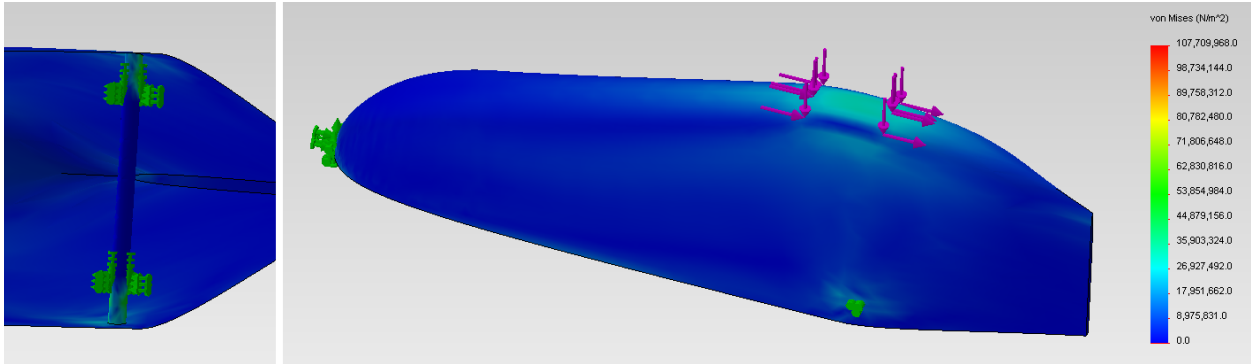


Figure 9: 600lb-f top loading, 12 degrees from vertical on the RPS. The maximum von Mises stress is well below the yield strength for both the bar and the shell.

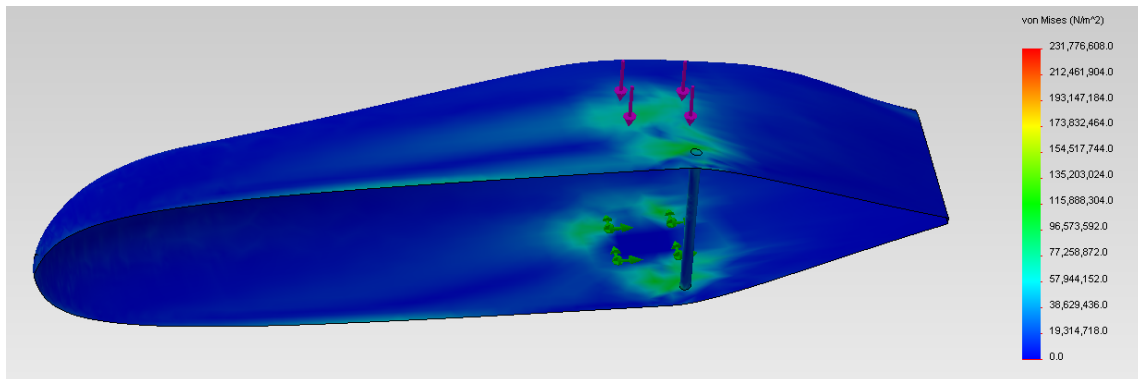


Figure 10: 300lb-f side loading on the RPS. Once again, the von Mises is well below the yield strength of both the bar and the shell.

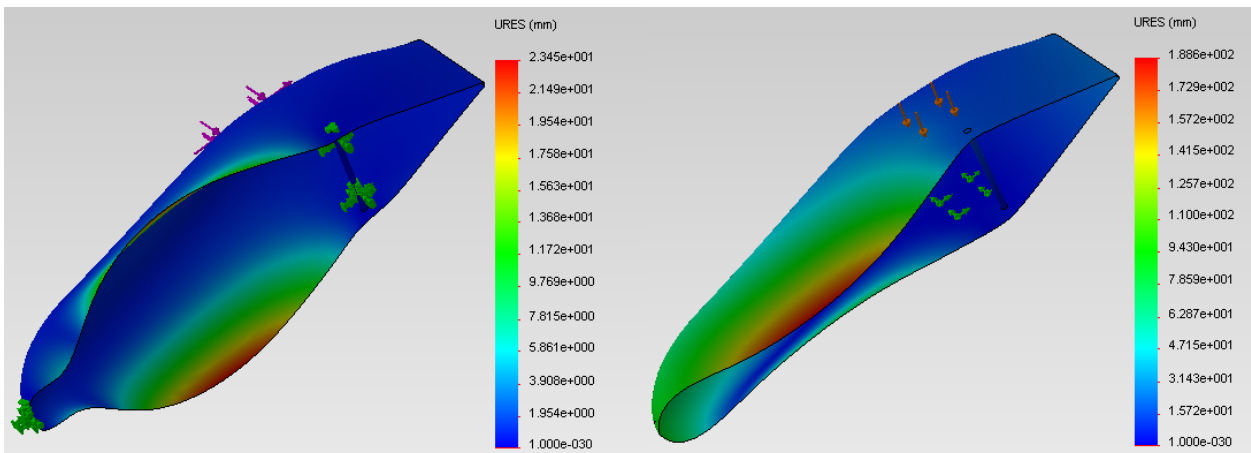


Figure 11: Displacement of the RPS under a top and side load (left and right respectively). The deformation in the side load case is above the allowable deformation limit, yet this model does not include ribbing that will be in the final model.

## Aerodynamics: Fairing Profile

We went into fairing design and analysis this year with the goal of testing numerous fairing shapes and iterating upon successful shapes to result in an optimized fairing design. We used CD-adapco's STAR-CCM+ Computational Fluid Dynamics simulation software, which we

began using last year, to analyze the different designs. We first identified five potential shape categories and made initial models of each to test in STAR-CCM+ with the intention of iterating upon the best shape.

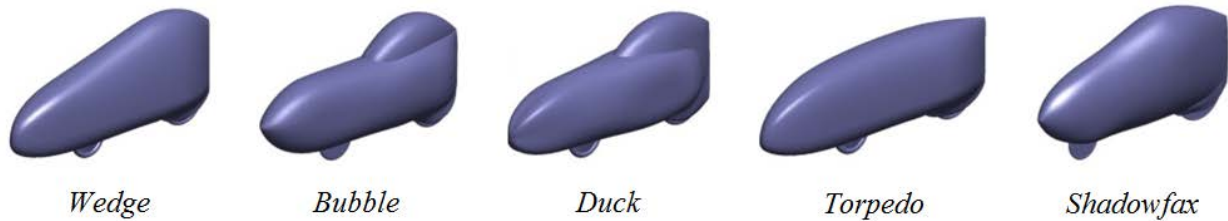


Figure 12: Fairing Shape concepts compared to Shadowfax, the 2011 competition vehicle.

In the simulations, we assumed a vehicle speed of 30mph including the ground moving at 30mph under the vehicle. Modeling the ground movement gives us more accurate measurements and prevents inaccurate deflation of drag coefficients. Wheels were modeled as solid bodies, representing the vehicle's wheel disks.

Fairing performance depends on low drag force, which is a function of drag coefficient, frontal area, air density and velocity. By factoring out the constants, we can compare our fairings on the metric of  $C_dA$  (drag coefficient times area):

$$C_dA = \frac{2F_D}{\rho v^2}$$

Calculating values based off simulated values of  $F_D$ , density of air as  $1.2 \frac{Kg}{m^3}$ , and a fluid velocity  $v$  of 30mph, Table 3 shows the  $C_dA$  values for *Shadowfax* and the design candidates:

<b>Wedge</b>	0.1098	0.428	0.0470
<b>Bubble</b>	0.1421	0.423	0.0601
<b>Duck</b>	0.1149	0.424	0.0487
<b>Torpedo</b>	0.1257	0.347	0.0436
<b>Shadowfax</b>	0.0743	0.551	0.0409

Table 3: Drag Force and  $C_dA$  Values for Candidate Fairings.

The simulation showed us that all of our fairing candidates were worse than *Shadowfax*. However, we decided that by iterating upon the better designs, we could potentially design a more aerodynamic fairing than our previous fairing. The Wedge and Torpedo were the two candidates which showed the most promise and we conducted a weighted objectives breakdown of the two designs and decided to move forward with the *Wedge* design. The *Wedge*, similar in shape to *Shadowfax*, exhibits excellent aerodynamic properties. Although *Torpedo* has a lower  $C_dA$  value than *Wedge*, it was decided that *Torpedo*'s low shape would negatively impact rider visibility, safety and confidence, adversely affecting the performance of the vehicle.

## 2D Testing

A full 3D STAR-CCM+ CFD analysis using our hardware takes at least 30 minutes, making full fairing analyses tedious and quick iteration difficult. To determine general aerodynamic design principles, we used 2D cross-sectional tests which could be run within a few minutes.

Performing 2D tests allowed us to run parameter sweeps on a variety of shape determining variables including tail concavity, length division between tail and head, and overall length. It was not necessary to test differing widths due to the width being well tied to frontal area and fairing mass, encouraging us to always minimize it (weighing it only against rider comfort). By performing 2D analysis, we were able to gain insight into what modifications to the *Wedge* concept would help decrease the drag coefficient.

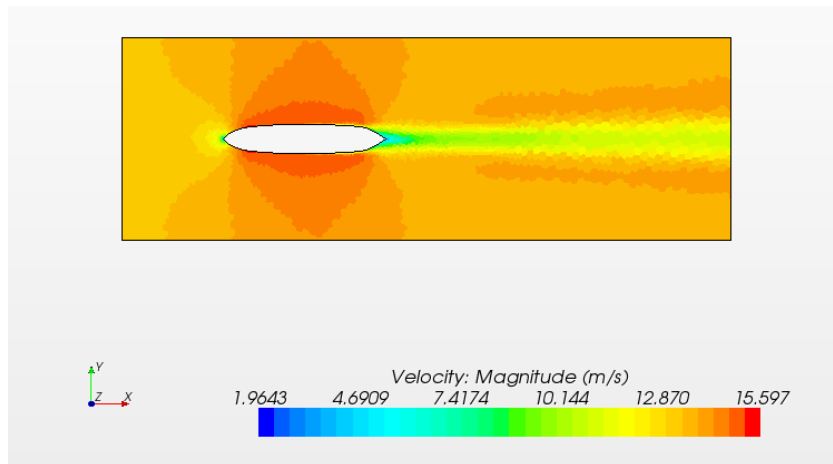
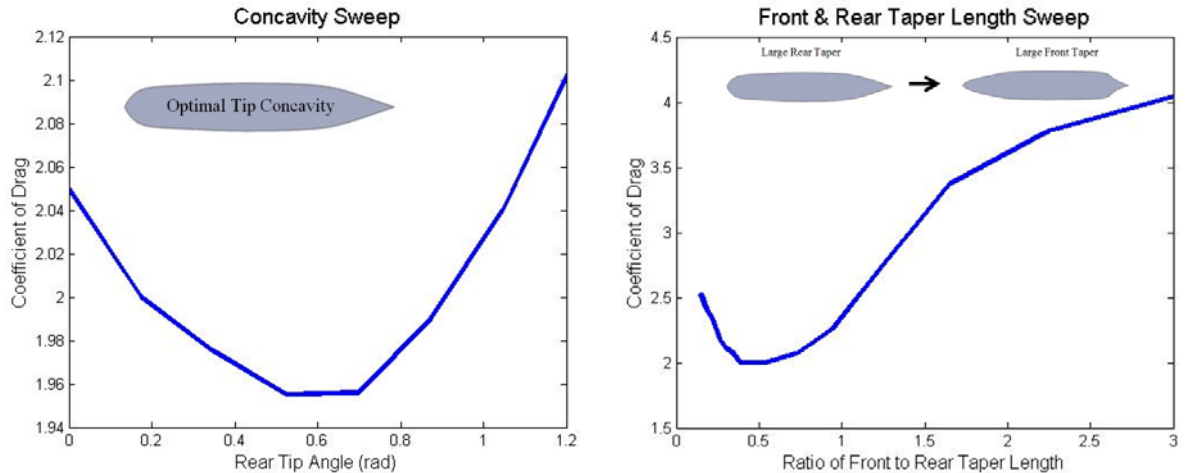


Figure 13: STAR-CCM+ 2D Simulation Result. 2D tests clearly show variations in cross-sectional design.

Tail shape has a large effect on aerodynamic performance. For a given length and starting width, the largest remaining shape defining variable is the concavity of the tail. For this test, we conducted a parameter sweep, varying the angle of the rear point of the fairing which defines the concavity of the taper spline.





Figures 14 and 15: Results of the concavity and taper proportion sweeps. As shown, the concavity defined by a rear tip angle of approximately 0.6 radians produces an optimal drag coefficient, and the optimal taper proportions have the front taper at about half the length of the rear taper.

We found that a very slightly concave tail produced the best drag results (approximately 35 degrees). Extremes in either direction have mediocre performance.

We designed our fairing around a rider box which contains the rider's limiting dimensions (shoulder and hip width) and the space needed for the various mechanisms (drivetrain, landing gear). The purpose of the fairing was to enclose this box in an aerodynamic shell with a constant length. We conducted a parameter sweep of relative length of the front and rear tapers while keeping overall length consistent and keeping concavity at the optimal angle shown from the last test. Results from this test encourage us to have the length devoted to tail area be approximately twice that of the head length.

Increasing fairing length allows us to craft smoother (and more aerodynamic) curves, but additional length increases material quantity and weight rise while making the fairing more difficult to transport and more susceptible to crosswinds. We conducted a parameter sweep to analyze the effect of fairing length on drag coefficient. The ratio of front to rear taper length and concavity were held constant at the values determined in the previous tests.

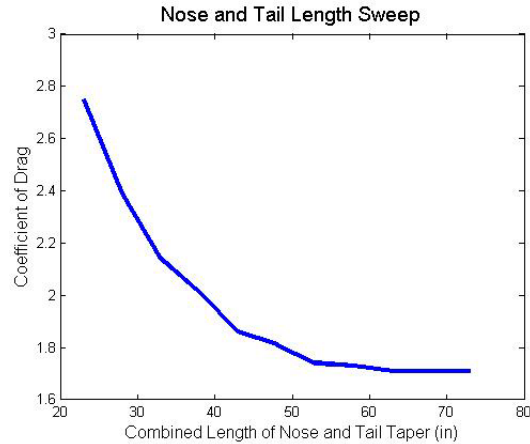


Figure 16: Results of the Fairing Length Sweep. As shown, as the length of the fairing gets longer, the coefficient of drag asymptotically reaches a limit of about 1.7.

We decided on an overall length of 8.5 feet because it provided significant aerodynamic improvements over shorter lengths while still maintaining an easily transportable length given our trailer size.

### *Iterating upon Wedge*

To improve the performance of the wedge design, several iterations were made. The length and taper shapes were modified to reflect the results of the 2D testing. Furthermore, wheel boxes were added to improve the aerodynamics of the wheels. The results of iterating upon the *Wedge* are shown in the table below. As shown, the final wedge has a  $C_dA$  value significantly lower than both the original wedge and *Shadowfax*, leading us to choose it as the fairing to build.

Vehicle	$C_d$	A (m <sup>2</sup> )	$C_dA$ (m <sup>2</sup> )
Original Wedge	0.1098	0.428	0.0470
Final Wedge (Seabagel)	0.0870	0.411	0.0358
Shadowfax	0.0743	0.551	0.0409

Table 4: Results of Iterating upon the Wedge Design.

To support the numerical results, we viewed the air patterns over the center line of the both the new *Seabagel* fairing and *Shadowfax*.

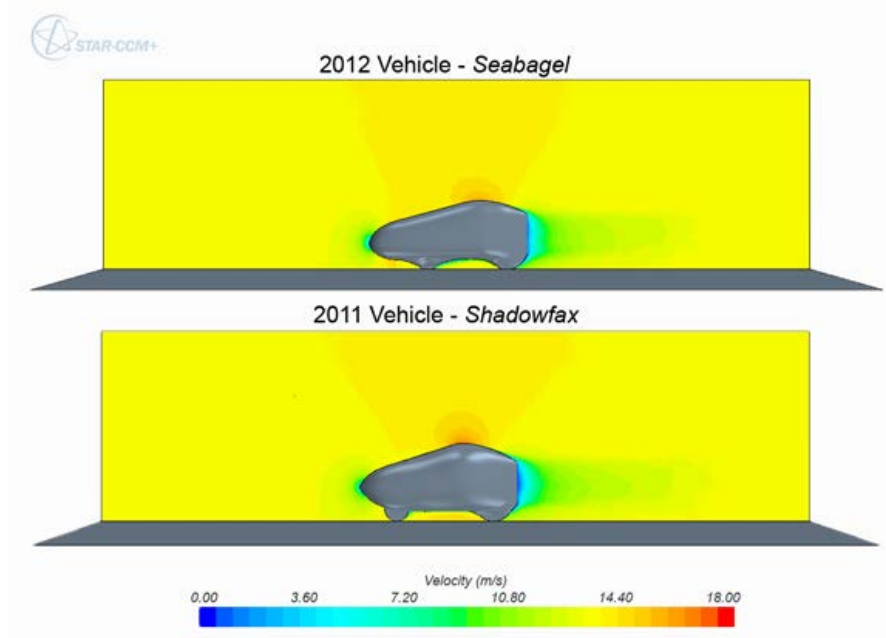


Figure 17: Fluid Velocity Profiles for Competition Vehicles. The 2012 vehicle is shorter and has smoother curves. Less air is trapped behind the vehicle and the low pressure pocket over the vehicle is diminished.

### Crosswind Analysis

To assure that the vehicle would be operable in a crosswind, a crosswind simulation was performed in STAR-CCM+. With the simulated side forces from STAR-CCM+, the fairing lean angle into the wind necessary to keep the vehicle upright was calculated.

$$\theta = \text{atan}\left(\frac{F_{drag}}{mg}\right)$$

Vehicle	Fdrag (N)	m (lb)	$\theta$
Seabagel	283	200	17.7°
Shadowfax	344	230	18.6°

Table 5: Side force on the vehicle due to a 10mph crosswind with a 30mph vehicle speed.

As shown, the necessary lean angle is less on *Seabagel* than on *Shadowfax*. Because we are confident that *Shadowfax* is operable in a crosswind, we are confident that *Seabagel* will be as well.

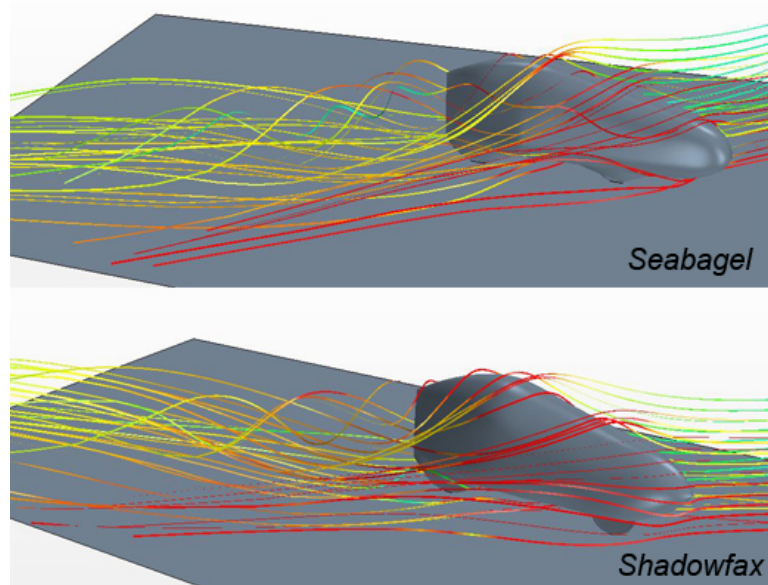


Figure 18: Results of Crosswind Simulations on Seabagel and Shadowfax.

As demonstrated by the simulation, the turbulence created by the fairings in a crosswind is very similar in the two fairings, due to their similar shapes. However, *Seabagel* has a lower profile to the ground and the air velocities stay lower.

## Interchange Strength Analysis

In previous years, we had modified a rear hub to act as the interchange between our first and second chain runs. In an attempt to narrow this junction, which lies directly between the rider's legs during vehicle operation, we designed our own interchange. For simplicity of fabrication, we chose to make the interchange hub, seen in Figure 19(a), out of 6061 aluminum. However, because most cassette bodies are made from stainless steel, we feared the rider could possibly distort the aluminum when a stalled torque was exerted.

To allay these fears, we used the SolidWorks Simulation Finite Elemental Analysis (FEA) package to evaluate potential for failure. Based on previous calculations, we estimated that a 400lb-f load is the maximum that any of our riders could exert. The FEA confirmed that twice this load, applied at both pedals and distributed equally over eight teeth, is safe. The FEA analysis results are shown in Figure 19(b).

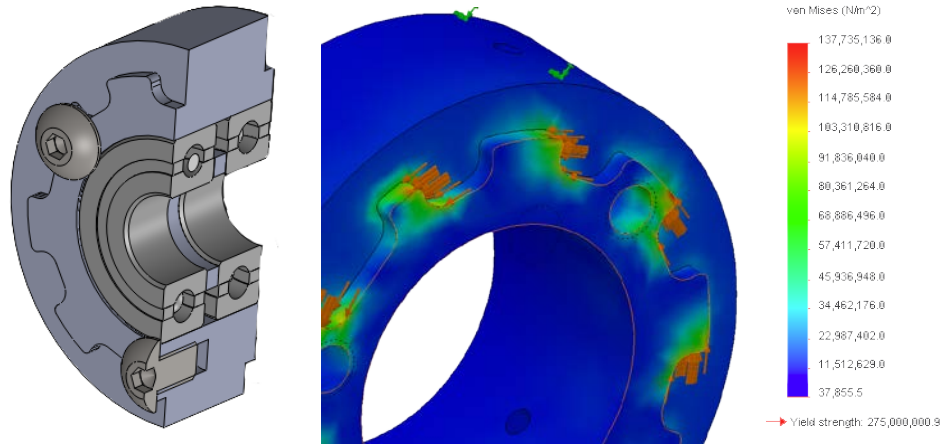


Figure 19: (a) cut-away view with bearing separation spacer, and (b) FEA results.

## Testing

### Rollover Protection System

No matter the high level of trust we place in FEA, as verified by our previous experience with standard materials, analysis of composites creates an abstraction away from the real world in assuming uniform construction. This major flaw can produce erroneous results which, given the implicit relationship between our rollover protection system and rider safety, necessitates that we perform real-world testing. Specifically worrisome is the crumpling and intense deflection we know composite construction can undergo, both of which would endanger our riders.

In order to alleviate our doubts, we performed destructive testing with an Instron stress-strain machine on the top half of a 1/3 scale fairing.

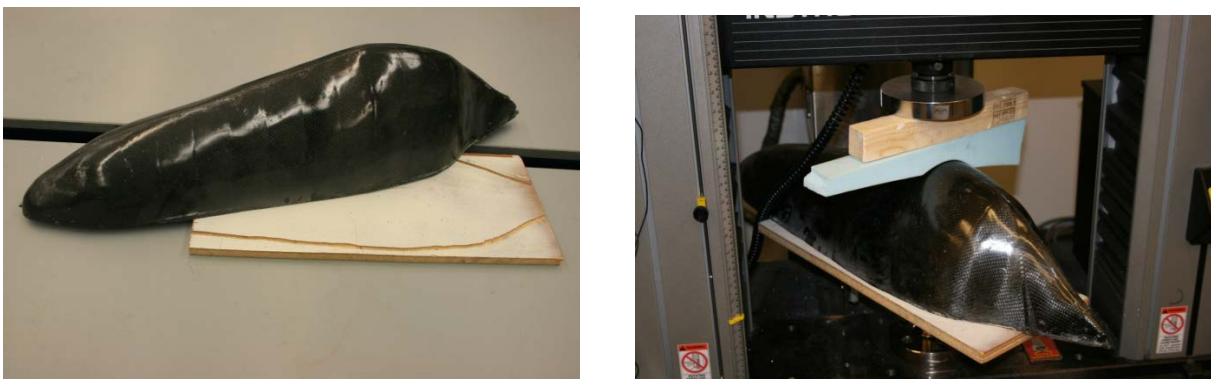


Figure 20:(a) Scale fairing before test resting on test jig. A router was used to produce the edge constraining channels, and (b) testing set-up immediately before displacement test.

Because we suspect that much of the strength in the top half of our scale fairing comes from its design, which constrains against splaying, we produced a test fixture to constrain the bottom edge and provide load to the highest point of the fairing.

We then performed destructive compression testing where we measured the load supported by the fairing top, shown in

Figure 22.



Figure 21:(a) Scale fairing showing deflection, and (b) fractured fiber failure point shown by white streaks.

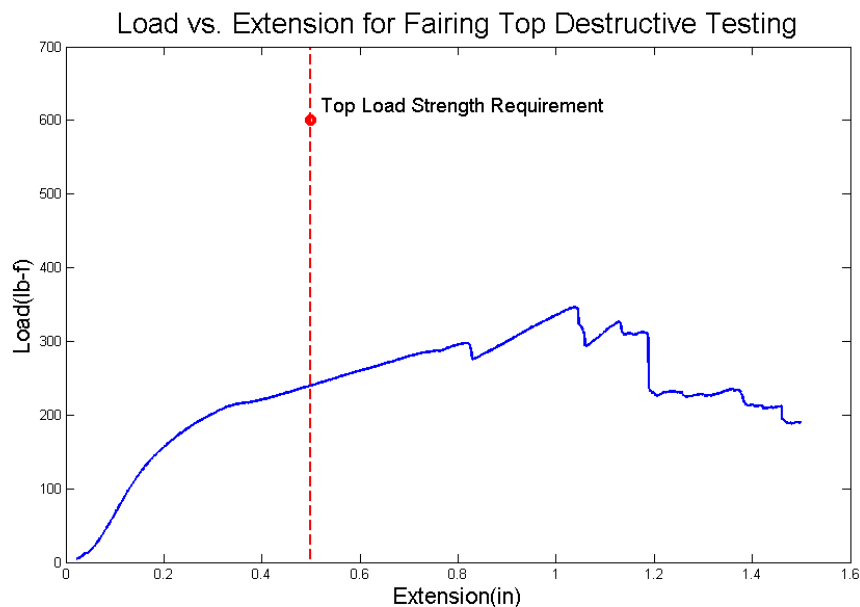


Figure 22: Instron Produced Plot Demonstrating Strength of Scale Fairing Top. Note: Failure to reach strength requirement necessitates serious reinforcement through ribbing and additional layers.

From this test, we concluded that the scale fairing did not support the mandated 600lb-f. While we do not know the scaling of what the yield force for a small fairing should be, we do know that it would need to support more than the 600lb-f requirement for the full size fairing. This test tells us that we need to re-evaluate our construction method. Because the main failure mode was buckling, we plan on re-enforcing the RPS in the areas of applied load to prevent buckling. We will perform more testing for the RPS once completed, to be included in the design report update.

## Developmental Testing

### Composite Rib Shape

The large surface of our fairing, much like that of a soda can, is most vulnerable to buckling conditions under concentrated loads. In order to distribute loads across the fairing's surface, we will install ribs. We tested a variety of ribs with different cross-sections to observe which had the greatest strength. The makeup of each rib can be seen in Figure 23.

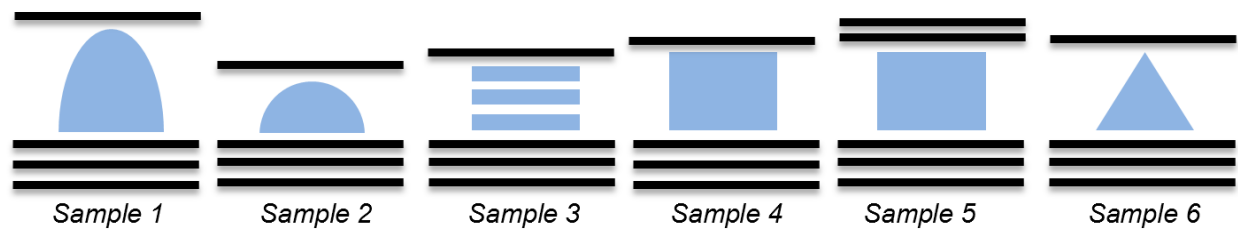


Figure 23: Cross sections of each tested composite rib. The black lines represent layers of carbon fiber on either side of the filler material. We used expanded polystyrene foam to provide the desired geometry.

To test the ribs' strength, we fixed each test rib in a three-point bend configuration and applied loads at the ribs' centers. Though the test fixture concentrates the load across a very narrow distance of the rib, we are using this data for comparative rather than absolute purposes. Because our composite analysis tools are not adequately suited to compute the fairing's resistance to buckling, we will use small-scale testing combined with qualitative assessment to size and position ribs across the fairing's surface. Destructive testing will provide strength comparisons, allowing us to design a rib with the optimal cross-sectional shape. By measuring strength as a function of flexural displacement, we acquired the results seen in Figure 24.

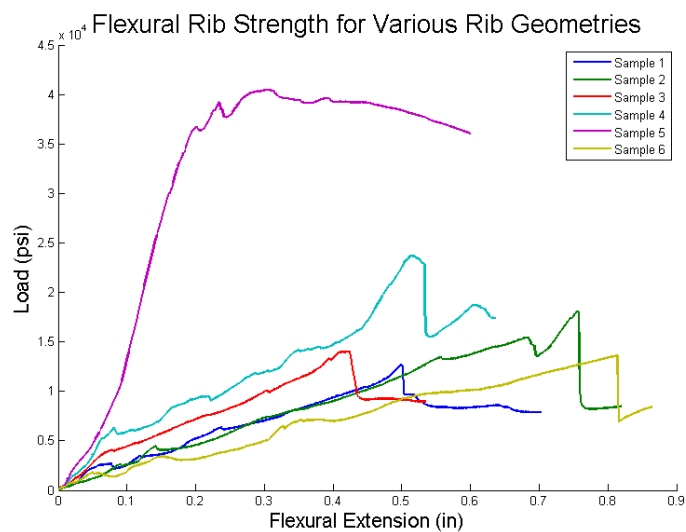


Figure 24: Rib strength for various geometries.

These results illustrate that applying two layers of carbon to a rib's top surface, as we did in Sample 5, will significantly increase its strength. It is also clear that maximizing a rib's cross-sectional area will supplement its resistance to bending, as predicted by the Euler-Bernoulli Equation:

$$EI \frac{d^4 w(x)}{dx^4} = F(x)$$

where  $I$  is the area moment of inertia,  $E$  is the elastic modulus of the material,  $w$  is the rib's displacement, and  $F$  is the applied load. Without using calculus, it is clear that increasing the cross-sectional area decreases the flexural displacement. This also meets one's intuition regarding static systems.

The differences in strength between Samples 3 and 4 show the difference between solid ribs and layered ribs. The layered ribs are incapable of transmitting shear stresses across the interfaces between the ribs. This transverse shifting makes layered ribs less resistant to flexure. However, layered ribs are often easier to fabricate. In sections where layered ribs are necessary, we will increase carbon reinforcement and rib thickness to account for the weakness. Our understanding of the ribs' load-bearing characteristics will allow us to better distribute ribs to maximize strength on both a per-weight and per-labor basis.

### *Rider Confidence Testing*

The purpose of this test was to determine if differences in rider confidence have a noticeable effect on rider speed in a fully-faired recumbent vehicle. This question was motivated by an observed discrepancy at the 2011 HPVC between the members of our team who had higher levels of physical fitness and members who rode fastest

If rider confidence has no significant effect on rider speed, then we would expect to see speed increase as power increases. If rider speed is instead significantly influenced by rider confidence, then we would expect to see little or no correlation between rider power and speed.

All riders operated the same vehicle using a full fairing under similar race conditions. Speed was measured by timing riders around a 0.47 mile course that included a total elevation change of 50 feet and had 3 technical turns.

Power was measured using a custom-built rig where a rider in a recumbent position powered an electric motor. This motor was loaded with a known resistance, and we measured the voltage drop across this resistor. Knowing that  $P = v^2/R$ , we used our measured values to calculate the power. This power measurement does not capture the mechanical and electrical power losses elsewhere in the system. This does not affect the usefulness of the results because all power draws on the rig increase with pedal cadence, and thus a larger power dissipated by the resistor will still correlate to a more powerful rider. The test was to exert as much power as possible over a 90-second interval, which is a comparable time frame to the duration of the speed test.



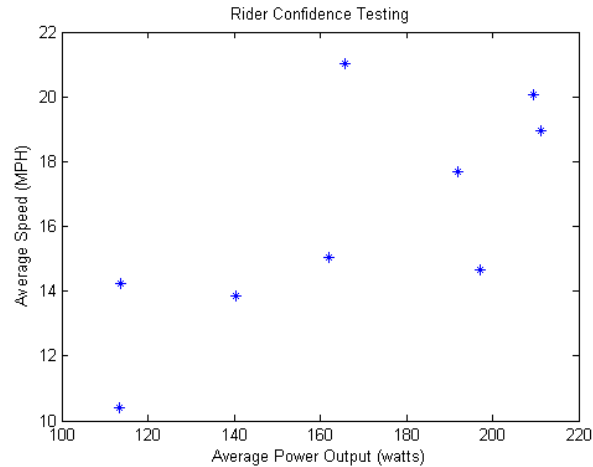


Figure 25: Rider speed vs. power output

We measured the power and speed of twelve riders, whose results can be found in Figure 25. For many riders, this was their first time riding in a fully faired vehicle. Most of the riders are concentrated around two speed zones independent of power, one around 14mph and one around 20mph. The riders in the 14mph grouping are largely riders who had logged the least amount of time and the riders in the 20mph grouping were our most experienced riders. Most notably, our fastest rider was not our most powerful rider, yet he is unanimously considered our most experienced rider.

A Pearson correlation between the average power and average speed of these riders was not significant,  $r = 0.598$ ,  $p > 0.05$ . This suggests that there are other variables that contribute to a rider's speed, and rider's confidence may play a key role in this. To confirm this, a point-biserial correlation was run, where new riders (first-years) were operationally defined as riders with no experience, and sophomores, juniors, seniors, and alumni were operationally defined as riders with experience. The correlation between average power and rider experience was not significant:  $r = 0.308$ ,  $p > 0.05$ . The correlation between average speed and rider experience was significant,  $r = 0.725$ ,  $p < 0.05$ . These relationships point to a strong relationship between speed and rider experience, and a weaker one between power and speed. This indicates that it is useful to consider rider experience when looking for a faster rider.

This testing highlights that the vehicle and rider need to be considered as an entire system during design. Decisions that may appear to have a theoretical increase in maximum speed may result in a decrease in realized speed if they decrease the ridability of the vehicle. Furthermore, these results highlight that if we want to increase our vehicle and rider performance at competition, we should focus on confidence training before we focus on strength training.

## Performance Testing

### *Interchange Strength Testing*

To back up the analysis on the strength of the interchange between our first and second chain runs, we created a rig to apply torque at a cog. This rig consisted of a partially-machined cog

bolted to a sprocket. We held the sprocket motionless and used a fixture to apply a moment. The test interchange hub, along with deformed post-testing results, can be seen in *Figure 26*.

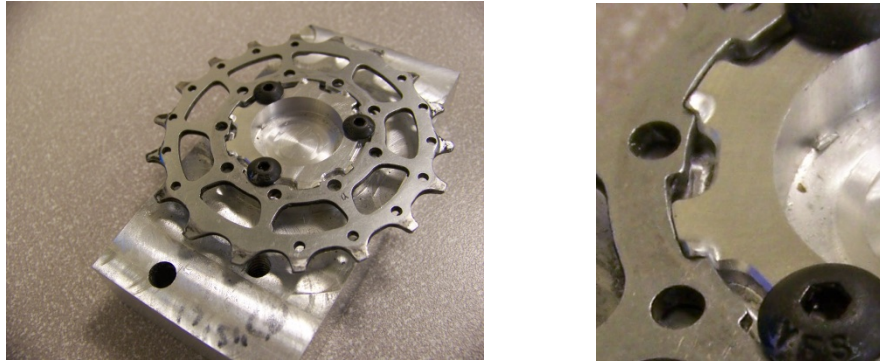


*Figure 26: (a) Testing setup for the interchange and (b) close-up of deformation.*

We found that the teeth on the interchange hub deformed at an applied load of 145ft-lbs. With this number we calculated the force a rider would have to apply to deform the hub:

$$F_{applied} = \frac{\tau_{fail}}{L_{crank}} * R$$

Substituting in our crank length ( $L_{crank}$ ) of 160mm (.52ft), our failure torque ( $\tau_{fail}$ ) of 145ft-lbs, and our gear ratio (R) of 53/11, we find that a rider would have to exert 1300lbs of force to deform the interchange hub, a value significantly higher than the force output of even our strongest rider.

This value is closely correlated with the value predicted by FEA analysis. However, our experimental data provides a higher yield strength because we deformed our interchange hub considerably more than the 0.2% deviation from elastic deformation use to define yield strength.

### *Rider Adjustment Testing*

We wanted to test the new crank adjustment system on the vehicle to see how quickly it could be operated. To do this, we measured the time that it took three different people to adjust the cranks on *Seabagel* and compared this to the times that it took them to adjust the seat on other vehicles. These other vehicles had various ways of adjusting the seats, as described below.

Vehicle	Adjustment Method	Adjustment Time (Seconds)			
		Person 1	Person 2	Person 3	Average
<i>Seabagel</i>	Crank Adjustment System	10.53	14.90	6.59	10.67
<i>Blues Wagon</i>	Moveable Clamps Underneath Seat	9.4	14.08	9.29	10.92
<i>Bucephalus</i>	Single Pin with	8.65	9.13	4.02	7.27

	Holes Behind Seat				
<i>Shadowfax</i>	Two Pins with Holes on Either Side of the Seat	15.87	19.74	10.81	15.47

*Seabagel's* crank adjustment system is comparable to the different methods of seat adjustment that are on the other vehicles in terms of the time that it takes to adjust it. It outperformed *Blues Wagon's* and *Shadowfax's* seat adjustment system, but it was a bit slower than *Bucephalus's* single pin system. The high reliability and fairly quick adjustment time confirms that this new crank system is acceptable for competition.

## **Safety**

*Seabagel* was designed to provide a safe environment for all drivers and bystanders. Our focus on adjustability and ridability ensures that each of our drivers has the confidence and ability to ride *Seabagel* comfortably and securely.

In years past our roll bar was designed so that the tallest riders were comfortably inside of it, but because of our sliding seat, the shortest riders were positioned in front of the roll bar. This year we ameliorated that situation with a static seat and adjustable cranks. Each rider's torso is now in the same position regardless of their height, ensuring that each rider is afforded the benefit provided by the RPS. In addition to a non-mobile seat, a commercial four-point safety harness is included which ensures that the driver remains safely in the seat during a crash. The area around the rider's head and helmet will be padded so that the rider does not experience a sharp blow in the event of a rollover.

In addition to implementing a comprehensive roll protection system, our full fairing protects our riders from contacting rough surfaces, preventing abrasion. The area around the rider's shoulders has added thickness for added rollover protection as this is expected to be one of the primary points of contact. This area is also lined on the interior with Kevlar, which helps protect the driver because it will bend rather than splinter.

Although it is important that the full fairing remains closed during the duration of a crash in order for the RPS to work correctly, it is also important that first responders are able to extract the rider from the vehicle in the unlikely event that the rider would be unable to activate the fairing top release mechanism. For this reason, the fairing top release mechanism has outer access holes to enable removal from the outside.

*Seabagel* is our first vehicle not designed for speed class, and as such it inherently must have additional safety features not found on our previous vehicles. The most important is the Slow Speed Stability System (SSSS); on previous vehicles if our rider slowed down too much while fully-faired, the driver had no ability to balance the vehicle. The SSSS enables drivers to easily stop and start on their own, avoiding the potential of becoming an obstruction to other vehicles on the course and reducing the number of simple fall-over events. *Seabagel* also has lights which increase both our rider's visibility of the course and other drivers' visibility of *Seabagel*.

While it is important that riders remain safe during the operation of the vehicle, it is of utmost importance that we as a team remain safe during the construction of the vehicle. Our team's accident-free record is due to our adherence to the safety procedures outlined by our school, as well as the use of intelligent decision making and proper safety procedures when performing tasks not explicitly covered under our school's safety procedures. This primarily involves following a buddy system and wearing appropriate PPE when machining or performing composite work, and making sure that team members have completed the proper training. In addition to these standard safety procedures, certain fabrication methods are favored because of their increased safety benefits. One example is the vacuum bagging technique used for layup, which decreases both the amount of time spent handling uncured epoxy and the amount of time spent sanding composite materials.

**Appendix****Appendix A. Cost Analysis**

	Quantity	Price	Unit	Total
<b>Frame</b>				
Thin Walled 4130 Steel Tubing 1.75" diameter	6	\$6.00	Per Foot	\$36.00
Thin Walled 4130 Steel Tubing 7/8" diameter	10	\$3.50	Per Foot	\$35.00
Thin Walled 4130 Steel Tubing 1.25" diameter	4	\$3.70	Per Foot	\$14.80
Welding Supplies	1	\$20.00	Lump Sum	\$20.00
Assorted Mounting Hardware	1	\$60.00	Lump Sum	\$60.00
			<b>Subtotal</b>	<b>\$129.80</b>
<b>Fairing Molds (one per month)</b>				
Epoxy Hardener	1	\$155.00	Per Gallon	\$155.00
Epoxy Resin	1	\$100.00	Per Gallon	\$100.00
Fiberglass mat	8	\$4.00	Per Yard	\$32.00
Fiberglass fabric	15	\$8.00	Per Yard	\$120.00
Coroplast (4' x 8')	0.5	\$18.25	Per Sheet	\$9.13
XPS Blue Foam (2' x 8')	26	\$14.35	Per Sheet	\$373.10
Assorted composites tools	1	\$50.00	Lump Sum	\$50.00
Vacuum Bagging Supplies	1	\$122.00	Lump Sum	\$122.00
Vacuum Pump	1	\$110.00	Per Pump	\$110.00
			<b>Subtotal</b>	<b>\$1,071.23</b>
<b>Fairing</b>				
Epoxy Hardener	1.5	\$155.00	Per Gallon	\$232.50
Epoxy Resin	1.5	\$100.00	Per Gallon	\$150.00
Carbon Fiber Cloth	15	\$8.40	Per Yard	\$126.00
Assorted Composites Tools	1	\$50.00	Lump Sum	\$50.00
Vacuum Bagging Supplies	1	\$122.00	Lump Sum	\$122.00
PETG (4' x 4' x 1/16")	1	\$46.00	Per Sheet	\$46.00
			<b>Subtotal</b>	<b>\$726.50</b>
<b>Drivetrain</b>				
Derailleur	1	\$50.00	Per Unit	\$50.00
Wheels	2	\$100.00	Per Wheel	\$200.00
Crankshaft Steel	1	\$15.00	Per Unit	\$15.00
Crankshaft Bearing	4	\$25.00	Per Unit	\$100.00
Aluminum Crank	1	\$15.00	Per Unit	\$15.00
Chains	2	\$20.00	Per Unit	\$40.00
Interchange Sprockets	2	\$15.00	Per Unit	\$30.00
Pedals	1	\$35.00	Per Set	\$35.00
Aluminum Connector	1	\$15.00	Per Set	\$15.00
Various nuts and bolts	1	\$10.00	Lump Sum	\$10.00
Disc Brakes	1	\$50.00	Per Set	\$50.00
			<b>Subtotal</b>	<b>\$560.00</b>
<b>Seat</b>				
XPS Blue Foam	1	\$14.35	Per Sheet	\$14.35
Epoxy Hardener	0.125	\$155.00	Per Gallon	\$19.38
Epoxy Resin	0.125	\$100.00	Per Gallon	\$12.50
Fiberglass cloth	2	\$8.00	Per Yard	\$16.00
			<b>Subtotal</b>	<b>\$62.23</b>
<b>Labor Per Month</b>				
Machinist/Welder	3	\$3,200.00	Per Month	\$9,600.00
Composite Technician	3	\$2,080.00	Per Month	\$6,240.00
Floor Worker	4	\$1,600.00	Per Month	\$6,400.00
Manager	1	\$4,800.00	Per Month	\$4,800.00
			<b>Subtotal</b>	<b>\$27,040.00</b>

**Component Cost Per Vehicle**

Cost Savings Factor for Bulk Purchase	50%			
Drivetrain Components	10	\$280.00	Per Vehicle	\$2,800.00
Frame	10	\$64.90	Per Vehicle	\$649.00
Fairing	10	\$363.25	Per Vehicle	\$3,632.50
Seat	10	\$31.11	Per Vehicle	\$311.13
			<b>Subtotal</b>	<b>\$7,392.63</b>

**Monthly Overhead Costs**

Building Rental		\$1,500.00	Per Month	\$1,500.00
Utilities		\$400.00	Per Month	\$400.00
Welder Operating Costs		\$20.00	Per Month	\$20.00
Fairing Mold Cost		\$535.61	Per Month	\$535.61
			<b>Subtotal</b>	<b>\$2,455.61</b>

**Equipment (Single Purchase)**

CNC Router		\$15,000.00	Initial Purchase	\$15,000.00
Mill 1		\$22,000.00	Initial Purchase	\$22,000.00
Lathe 1		\$20,000.00	Initial Purchase	\$20,000.00
Grinder 1		\$150.00	Initial Purchase	\$150.00
Welder 1		\$3,500.00	Initial Purchase	\$3,500.00
Band Saw 1		\$2,000.00	Initial Purchase	\$2,000.00
Frame Jig 1		\$150.00	Lump Sum	\$150.00
			<b>Initial Purchase</b>	
			<b>Total</b>	<b>\$62,800.00</b>

Vehicles per Month	Months	Total Cost	Cost per Vehicle
10	<b>1</b>	\$99,688.24	<b>\$9,968.82</b>
10	<b>3</b>	\$173,464.71	<b>\$5,782.16</b>
10	<b>6</b>	\$284,129.43	<b>\$4,735.49</b>
10	<b>12</b>	\$505,458.85	<b>\$4,212.16</b>
10	<b>24</b>	\$948,117.70	<b>\$3,950.49</b>
10	<b>36</b>	\$1,390,776.55	<b>\$3,863.27</b>

## **Appendix B. Engineering Drawings**